The Astrophysical Journal, 667:358–366, 2007 September 20

MAGIC UPPER LIMITS ON THE VERY HIGH ENERGY EMISSION FROM GAMMA-RAY BURSTS

J. Albert,[1] E. Aliu,[2] H. Anderhub,[3] P. Antoranz,[4] A. Armada,[2] C. Baixeras,[5] J. A. Barrio,[4] H. Bartko,[6] D. Bastieri,[7] J. Becker,[8] W. Bednarek,[9] K. Berger,[1] C. Bigongiari,[7] A. Biland,[3] R. K. Bock,[6,7] P. Bordas,[10] V. Bosch-Ramon,[10] T. Bretz,[1] I. Britvitch,[3] M. Camara,[4] E. Carmona,[6] A. Chilingarian,[11] S. Ciprini,[12] J. A. Coarasa,[6] S. Commichau,[3] J. L. Contreras,[4] J. Cortina,[2] M. T. Costado,[13] V. Curtef,[8] V. Danielyan,[11] F. Dazzi,[7] A. De Angelis,[14] C. Delgado,[13] R. de los Reyes,[4] B. De Lotto,[14] E. Domingo-Santamaría,[2] D. Dorner,[1] M. Doro,[7] M. Errando,[2] M. Fagiolini,[15] D. Ferenc,[16] E. Fernández,[2] R. Firpo,[2] J. Flix,[2] M. V. Fonseca,[4] L. Font,[5] M. Fuchs,[6] N. Galante,[6] R. García-López,[13] M. Garczarczyk,[6] M. Gaug,[7] M. Giller,[9] F. Goebel,[6] D. Hakobyan,[11] M. Hayashida,[6] T. Hengstebeck,[17] A. Herrero,[13] D. Höhne,[1] J. Hose,[6] C. C. Hsu,[6] P. Jacon,[9] T. Jogler,[6] O. Kalekin,[17] R. Kosyra,[6] D. Kranich,[3] R. Kritzer,[1] A. Laille,[16] T. Lenisa,[14] P. Liebing,[6] E. Lindfors,[12] S. Lombardi,[7] F. Longo,[14] J. López,[2] M. López,[4] E. Lorenz,[3,6] P. Majumdar,[6] G. Maneva,[18] K. Mannheim,[1] O. Mansutti,[14] M. Mariotti,[7] M. Martínez,[2] D. Mazin,[6] C. Merck,[6] M. Meucci,[15] M. Meyer,[1] J. M. Miranda,[4] R. Mirzoyan,[6] S. Mizobuchi,[6] A. Moralejo,[2] K. Nilsson,[12] J. Ninkovic,[6] E. Oña-Wilhelmi,[2] N. Otte,[6] I. Oya,[4] D. Paneque,[6] M. Panniello,[13] R. Paoletti,[15] J. M. Paredes,[10] M. Pasanen,[12] D. Pascoli,[7] F. Pauss,[3] R. Pegna,[15] M. Persic,[14,19] L. Peruzzo,[7] A. Piccioli,[15] M. Poller,[1] E. Prandini,[7] N. Puchades,[2] A. Raymers,[11] W. Rhode,[8] M. Ribó,[10] J. Rico,[2] M. Rissi,[3] A. Robert,[5] S. Rügamer,[1] A. Saggion,[7] A. Sánchez,[5] P. Sartori,[7] V. Scalzotto,[7] V. Scapin,[7] R. Schmitt,[1] T. Schweizer,[6] M. Shayduk,[6,17] K. Shinozaki,[6] S. N. Shore,[20] N. Sidro,[2] A. Sillanpää,[12] D. Sobczynska,[9] A. Stamerra,[15] L. S. Stark,[3] L. Takalo,[12] P. Temnikov,[18] D. Tescaro,[2] M. Teshima,[6] N. Tonello,[6] D. F. Torres,[2,21] N. Turini,[15] H. Vankov,[18] V. Vitale,[14] R. M. Wagner,[6] T. Wibig,[9] W. Wittek,[6] R. Zanin,[2] and J. Zapatero[5]

Received 2006 December 14; accepted 2007 May 22

ABSTRACT

During its first data cycle, between 2005 and the beginning of 2006, the fast repositioning system of the MAGIC telescope allowed the observation of nine different gamma-ray bursts as possible sources of very high energy γ-rays. These observations were triggered by alerts from *Swift*, *HETE-2*, and *INTEGRAL*; they started as quickly as possible after the alerts and lasted for several minutes, with an energy threshold varying between 80 and 200 GeV, depending on the zenith angle of the burst. No evidence for gamma signals was found, and upper limits for the flux were derived for all events using the standard analysis chain of MAGIC. For the bursts with measured redshifts, the upper limits are compatible with a power-law extrapolation, when the intrinsic fluxes are evaluated taking into account the attenuation due to the scattering in the metagalactic radiation field.

Subject headings: gamma rays: bursts — gamma rays: observations

Online material: color figures

1. INTRODUCTION

The physical origin of the enigmatic gamma-ray bursts (GRBs) is still under debate, 40 years after their discovery (see Mészáros 2006 for a recent review). The possible detection of radiation in the very high energy (VHE) region (extending between a few tens of GeV and a few tens of TeV) will lead to a deeper understanding of the acceleration mechanisms and the emission processes from GRBs. The γ-ray emission observed by the Energetic Gamma Ray Experiment Telescope (EGRET) in some case extends up to the VHE band (Hurley et al. 1994; Dingus 1995; González et al. 2003), favoring the hypothesis of a highly relativistic source of nonthermal radiation situated in an optically thin region (Piran 1999); more insight, however, can be gained by a clear signal detection in the VHE region, or the evaluation of stringent upper limit in this energy band.

Several observations of GRBs at energies above 100 GeV have been attempted (Götting et al. 2003; Zhou et al. 2003), without showing any indication of a signal. This is due to relatively low sensitivity, as in satellite-borne detectors, or to high energy thresholds, as in the previous generation of Cerenkov telescopes or in particle detector arrays. Only a few tentative detections of radiation above 0.1 TeV were reported by MILAGRITO for GRB

[1] Universität Würzburg, D-97074 Würzburg, Germany.
[2] Institut de Física d'Altes Energies, Edifici Cn., E-08193 Bellaterra (Barcelona), Spain.
[3] ETH Zurich, CH-8093 Zurich, Switzerland.
[4] Universidad Complutense, E-28040 Madrid, Spain.
[5] Universitat Autònoma de Barcelona, E-08193 Bellaterra, Spain.
[6] Max-Planck-Institut für Physik, D-80805 München, Germany.
[7] Università di Padova and INFN, I-35131 Padova, Italy.
[8] Universität Dortmund, D-44227 Dortmund, Germany.
[9] University of Łódź, PL-90236 Lodz, Poland.
[10] Universitat de Barcelona, E-08028 Barcelona, Spain.
[11] Yerevan Physics Institute, AM-375036 Yerevan, Armenia.
[12] Tuorla Observatory, Turku University, FI-21500 Piikkiö, Finland.
[13] Instituto de Astrofisica de Canarias, E-38200 La Laguna, Tenerife, Spain.
[14] Università di Udine, and INFN Trieste, I-33100 Udine, Italy.
[15] Università di Siena, and INFN Pisa, I-53100 Siena, Italy.
[16] University of California, Davis, CA 95616-8677.
[17] Humboldt-Universität zu Berlin, D-12489 Berlin, Germany.
[18] Institute for Nuclear Research and Nuclear Energy, BG-1784 Sofia, Bulgaria.
[19] INAF/Osservatorio Astronomico and INFN Trieste, I-34131 Trieste, Italy.
[20] Università di Pisa, and INFN Pisa, I-56126 Pisa, Italy.
[21] ICREA and Institut de Cienciès de l'Espai, IEEC-CSIC, E-08193 Bellaterra, Spain.

970417a (Atkins et al. 2000), or by the GRAND array for GRB 971110 (Poirer et al. 2003).

Upper limits on the prompt or delayed emission of GRBs were also set by Whipple (Connaughton et al. 1997; Horan et al. 2007), MILAGRO (Atkins et al. 2005; Saz Parkinson et al. 2006a, 2006b, 2007), STACEE (Jarvis et al. 2005), and HEGRA AIROBICC (Padilla et al. 1998).

Imaging atmospheric Cerenkov telescopes (IACTs) of the latest generation achieve a better flux sensitivity and a lower energy threshold, and thus are better suited to detect VHE γ-rays; on the other hand, their small fields of view permit unguided observations only by virtue of serendipitous detection, and they have to rely on an external trigger, such as that provided by automated satellite link to the GRB Coordinates Network (GCN), which broadcasts the coordinates of events triggered and selected by dedicated satellite detectors.

Among the new Cerenkov telescopes, MAGIC (Mirzoyan 2005) is best suited for the detection of the prompt emission of GRBs, because of its low energy threshold, its large effective area, and in particular, its capability for fast slewing (Bretz et al. 2003). The low trigger threshold, currently 50 GeV at zenith, should allow the observation of GRBs even at large redshift, as lower energy radiation can effectively reach Earth without interacting much with the metagalactic radiation field (MRF). Moreover, in its fast-slewing mode, MAGIC can be repositioned within 30 s to any position on the sky; in case of a target-of-opportunity alert by GCN, an automated procedure takes only few seconds to terminate any pending observation, validate the incoming signal, and start slewing toward the GRB position. Until now, the maximal repositioning time has been $\sim$100 s. In two cases, this allowed the placement of upper limits on the GRB flux even during prompt emission (Galante et al. 2005; Albert et al. 2006; Morris et al. 2007).

The detection of VHE radiation from GRBs is important for comparing different theoretical models. Emission in the GeV–TeV range in the prompt and delayed phases is predicted by several authors (see Zhang & Mészáros 2001; Pe'er & Waxman 2004; Razzaque et al. 2004 for a detailed analysis). Possible processes comprise leptonic and hadronic models: inverse Compton (IC) scattering by electrons in internal (Papathanassoiu & Mészáros 1996; Pilla & Loeb 1998) or external shocks (Mészáros et al. 1994), IC in the afterglow shocks (Dermer et al. 2000; Zhang & Mészáros 2001; Derishev et al. 2001; Wang et al. 2001), IC by electrons responsible for optical flashes (Beloborodov 2005), pure electron-synchrotron (Zhang & Mészáros 2001) and proton-synchrotron emission (Totani 2000), photon-pion production (Waxman 1995; Böttcher & Dermer 1998; Chiang & Dermer 1999; Li et al. 2002; Fragile et al. 2004), and neutron cascades (Bahcall & Mészáros 2000; Derishev et al. 1999; Rossi et al. 2006).

During the early afterglow phase, the recent observations by the *Swift* satellite of X-ray flares lasting 10^3–10^5 s (Burrows et al. 2005) suggested an extended activity in the central engine of the GRB, and thus emission from late internal shocks (Kobayashi et al. 2007) or from refreshed shocks due to energy injections at later times (Guetta et al. 2007). In some cases, the energy release of these flares can be of the same order of magnitude as the energy release in the prompt phase, as reported for GRB 050502b. The possibility of correlated γ-ray emission extending into the GeV–TeV region is predicted as well, where the corresponding VHE flares are predicted to originate from IC-scattered photons in the forward shock (Wang et al. 2006). Thus, observation of the delayed activity is of particular interest, being in most cases not constrained by the alerting and slewing time, and being still connected to the investigation of the central engine dynamics.

Measurements in this energy range can be used to test all these competing models. However, as most of the observed GRBs occur at large redshift, strong attenuation of the VHE γ-ray flux is expected, as a result of the interaction with low-energy photons of the MRF (Nikishov 1961; de Jager & Stecker 2002). The knowledge of the redshift, therefore, is important for a precise interpretation (Mannheim et al. 1996).

In this article, we report on the analysis of data collected on several GRBs followed by MAGIC during their prompt-emission and early afterglow phases.

2. GAMMA-RAY ANALYSIS WITH THE MAGIC TELESCOPE

The Major Atmospheric Gamma Imaging Cherenkov (MAGIC) telescope (Mirzoyan 2005), located on the Canary Island of La Palma (2200 m above sea level, 28°45′ north, 17°54′ west), completed its commissioning phase in early fall 2004. MAGIC is currently the largest IACT, with a 17 m diameter tessellated reflector dish consisting of 964 0.5×0.5 m^2 diamond-milled aluminum mirrors. In its current configuration, the MAGIC photomultiplier camera has a trigger region of 2.0° diameter (Cortina et al. 2005) and a trigger collection area for γ-rays of the order of 10^5 m^2, which increases further with the zenith angle of observation. Presently, the accessible trigger energy range spans from 50–60 GeV (at small zenith angles) to tens of TeV. The MAGIC telescope is focused to 10 km distance, the most likely height at which a 50 GeV γ-ray shower has its maximum. The accuracy in reconstructing the direction of incoming γ-rays, the point-spread function (PSF), is about 0.1°, slightly depending on the analysis.

The reconstructed signals are calibrated (Gaug et al. 2005) and then cleaned of spurious backgrounds from the light of the night sky using two different image-cleaning procedures: one algorithm requiring signal exceeding fixed reference levels, and a second algorithm employing additionally the reconstructed information of the arrival time (Gaug 2006). Nonphysical background images are eliminated (e.g., car flashes having triggered the readout). Events are processed by means of the MAGIC standard analysis software (Bretz et al. 2005), using the standard Hillas analysis (Hillas 1985; Fegan et al. 1997). Gamma/hadron separation is performed by means of the random forest (RF) method (Breiman 2001), a classification method that combines several parameters describing the shape of the image into a new parameter called "hadronness" (Hengstebeck 2006), the final γ/hadron discriminator in our analysis. Monte Carlo samples are used to optimize, as a function of energy, the cuts in hadronness. The energy of the γ-ray is also estimated using an RF approach, yielding a resolution of $\sim$30% at 200 GeV. The parameter ALPHA of the Hillas analysis, which is related to the direction of the incoming shower, is not included in the calculation of hadronness, as it is used separately to evaluate the significance of a signal. If the telescope is directed at a point-like γ-ray source, as a GRB is expected to be, the ALPHA distribution of collected photons should peak at 0°, while it is uniform for isotropic background showers.

3. BLIND TEST WITH CRAB NEBULA

On 2005 October 11 at 02:17:37 UT, the *INTEGRAL* satellite announced GRB 051011[22] at the J2000.0 position R.A. = $5^h34^m47^s$, decl. = +21°54′39″. A few hours later, *INTEGRAL* sent a new GCN (Mereghetti & Mowlavi 2005) stating that GRB 051011 was in fact the Crab Nebula. Thus, in a blind test, we acquired 2814 s of events coming from the Crab Nebula, the standard

[22] IBAS alert 2673; see http://ibas.iasf-milano.inaf.it

TABLE 1
SUMMARY OF GRBs OBSERVED BY MAGIC FROM 2005 APRIL TO 2006 MARCH

Number	Burst	Satellite	T_0 (UT)	$\Delta T_{\rm alert}$ (s)	$\Delta T_{\rm start}$ (s)	$t_{\rm slewing}$ (s)	Data (minutes)	Zenith Angle (deg)
1.....	GRB 050421	*Swift*	04:11:52	58	108	26	75	~52
2.....	GRB 050502a	*INTEGRAL*	02:13:57	39	689	223	87	~30
3.....	GRB 050505	*Swift*	23:22:21	540	717	90	101	~49
4.....	GRB 050509a	*Swift*	01:46:29	16	131	108	119	~58
5.....	GRB 050713a	*Swift*	04:29:02	13	40	17	37	~49
6.....	GRB 050904	*Swift*	01:51:44	82	145	54	147	~24
7.....	GRB 060121	*HETE-2*	22:24:54	15	583	...	53	~48
8.....	GRB 060203	*Swift*	23:55:35	171	268	84	43	~44
9.....	GRB 060206	*Swift*	04:46:53	16	59	35	49	~13

NOTES.—Here $\Delta T_{\rm alert}$ stands here for the time delay after T_0 until the burst coordinates were received from the GCN; $\Delta T_{\rm start}$ is the total time delay before the observation could be started, of which $t_{\rm slewing}$ is the time lost for repositioning the telescope. Data column shows the total amount of data taken.

source of γ-rays at VHE energies. The analysis yielded a 14 σ signal above 350 GeV (Scapin et al. 2007), showing that MAGIC can observe, at 5 σ level, spectra of 5 crab (1 crab = 6.57×10^{-10} cm^{-2} s^{-1} above 100 GeV) of intensity in 40 s, if above 300 GeV, and in 90 s if below 300 GeV.

4. GRBs OBSERVED BY MAGIC DURING ITS FIRST OBSERVATION CYCLE

An automatic alert system has been operational from 2004 July 15. Since then, about 200 GRBs were detected by *HETE-2*, *INTEGRAL*, and *Swift*, out of which about 100 contained GRB coordinates. Time delays to the onset of the burst were of the order of several seconds to tens of minutes. During the first MAGIC data cycle, between 2005 April and 2006 March, nine GRBs were observed by MAGIC during the prompt or the early afterglow emission phase, as listed in Table 1. In two cases the prompt alerting by the GCN and the fast reaction of the MAGIC telescope allowed to take data not only on the early afterglow, but also on part of the prompt emission of the burst. These two bursts are GRB 0507013a and GRB 050904, and will be considered separately.

4.1. *The Properties of Observed GRBs*

Table 2 summarizes the properties of observed GRBs by MAGIC according to the information distributed through the GCN Circular service.

GRB 050421 was detected by the Burst Alert Telescope (BAT) on board *Swift* (Barbier et al. 2005a). The other telescope on board *Swift*, the X-Ray Telescope (XRT), observed the burst in the 0.2–10 keV range from $T_0 + 97$ s and detected two X-ray flares at $T_0 + 110$ and $T_0 + 154$ s (Godet et al. 2006). Figure 1 shows the X-ray light curve of this burst. It can be seen that the MAGIC observation window is overlapped with the XRT ones on the X-ray afterglow. In particular, the two small X-ray flares are in the observation window of MAGIC. No optical counterpart was observed; thus GRB 050421 has been cataloged as a dark burst.

GRB 050502a was triggered by *INTEGRAL*; no X-ray counterpart was observed, but an optical afterglow followed the burst (Gotz 2005a, 2005b; Durig 2005). GRB 050505 was triggered by BAT and its light curve presented three short spikes at $T_0 + 23.3$, $T_0 + 30.4$, and $T_0 + 50.4$ s (Hurkett et al. 2005a; Hullinger et al. 2005). Both X-ray and optical observations followed the burst, but there was no simultaneous observation by MAGIC and the other instruments on board the satellite, as shown in Figure 2.

GRB 050509a was triggered by BAT and later XRT detected an X-ray counterpart (Hurkett et al. 2005b; Barbier et al. 2005b). GRB 060121 is the only short burst observed by MAGIC and was triggered by *HETE-2* (Arimoto et al. 2006; Golenetskii et al. 2006). XRT observed the afterglow as well and detected a fading X-ray source inside the *HETE-2* error box (Mangano et al. 2006), as shown in Figure 3. Unfortunately, there is no overlap between MAGIC observation and XRT observation. An optical counterpart was not confirmed by TNG, which did detect, however, a weak source inside the XRT error box (Malesani et al. 2006). Moreover, *HST* gave no evidence of an optical afterglow, although the burst lay close to a faint red galaxy at high redshift (Levan et al. 2006).

TABLE 2
MAIN PROPERTIES OF GRBs OBSERVED BY MAGIC

Number	Burst	Trigger Number	Energy Range	T_{90} (s)	Fluence (erg cm^{-2})	z
1.....	GRB 050421	115135	15–350 keV	10	1.8×10^{-7}	...
2.....	GRB 050502a	2484	20–200 keV	20	1.4×10^{-6}	3.79
3.....	GRB 050505	117504	15–350 keV	60	4.1×10^{-6}	4.27
4.....	GRB 050509a	118707	15–350 keV	13	4.6×10^{-7}	...
5.....	GRB 050713a	145675	15–350 keV	70	9.1×10^{-6}	...
6.....	GRB 050904	153514	15–350 keV	225	5.4×10^{-6}	6.29
7.....	GRB 060121	4010	0.02–1 MeV	2	4.7×10^{-6}	...
8.....	GRB 060203	180151	15–350 keV	60	8.5×10^{-7}	...
9.....	GRB 060206	180455	15–350 keV	11	8.4×10^{-7}	4.05

NOTES.—The fourth column shows the typical energy range of the detector on board the satellite, while the fifth, sixth, and seventh columns show the corresponding measured duration T_{90}, fluence, and redshift.

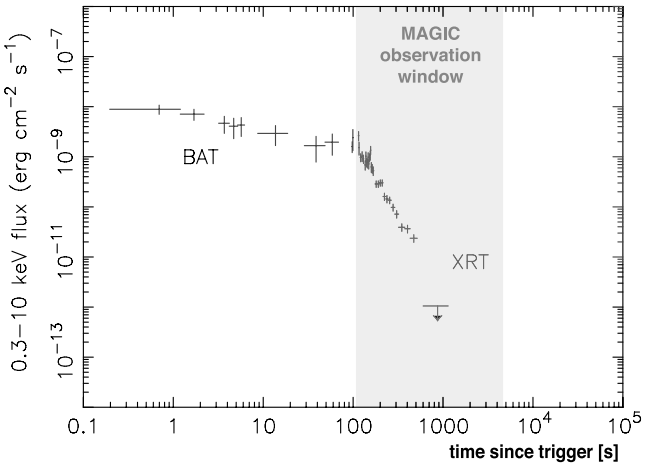

FIG. 1.—Flux of GRB 050421 measured by BAT and XRT. The shaded area represents the MAGIC observation time window and the overlap with *Swift* data. [*See the electronic edition of the Journal for a color version of this figure.*]

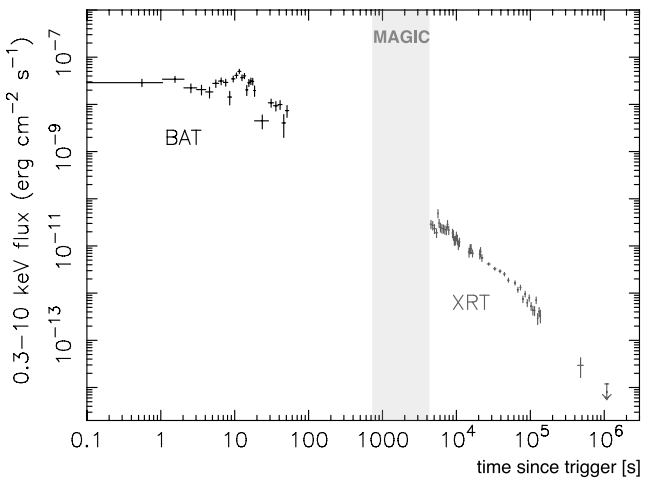

FIG. 2.—Flux of GRB 050505 measured by BAT and XRT. The shaded area represents the MAGIC observation time window, starting 717 s after the burst onset. [*See the electronic edition of the Journal for a color version of this figure.*]

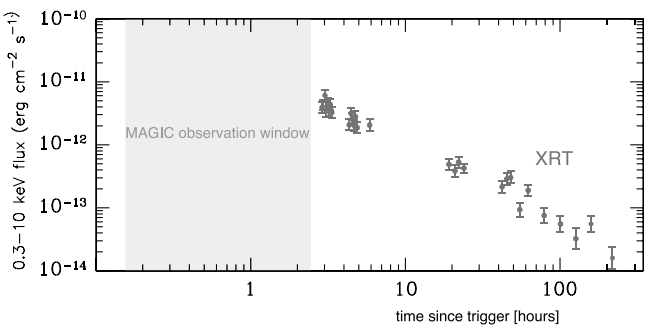

FIG. 3.—Flux of the afterglow of GRB 060121 measured by the *Swift* XRT detector. The MAGIC observation window is shown as shaded area. [*See the electronic edition of the Journal for a color version of this figure.*]

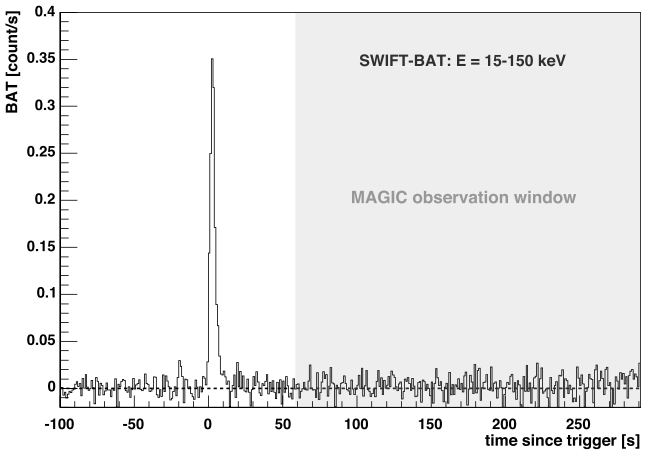

FIG. 4.—Light curve of GRB 060206 measured by BAT, sampled in bins of 1 s. The beginning of MAGIC observation is shown in the shaded area. [*See the electronic edition of the Journal for a color version of this figure.*]

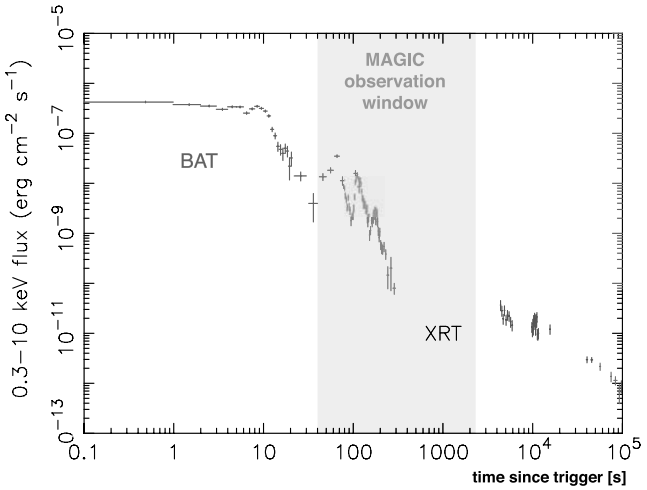

FIG. 5.—Flux of the prompt and afterglow emission of GRB 050713a measured by BAT and XRT. The shaded area illustrates the observation time window of MAGIC. [*See the electronic edition of the Journal for a color version of this figure.*]

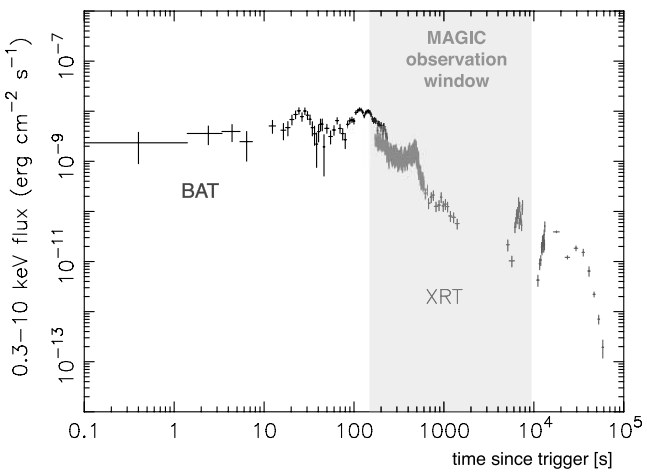

FIG. 6.—Flux measured by BAT and XRT in the prompt and afterglow emission of GRB 050904. The MAGIC observation window is shown in the shaded area. [*See the electronic edition of the Journal for a color version of this figure.*]

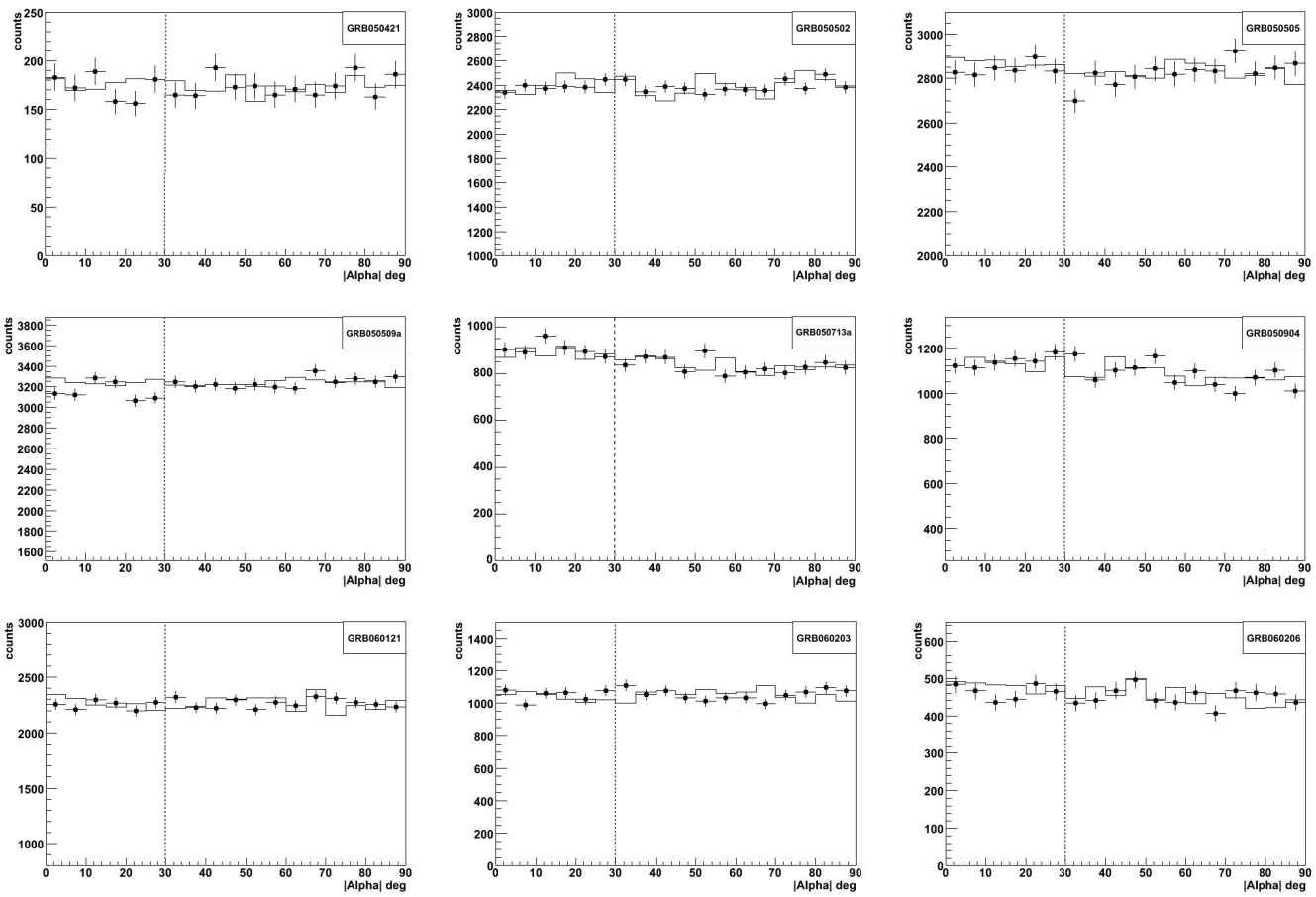

FIG. 7.—ALPHA plots of all nine GRBs for the complete data set of each burst. Points with error bars refer to the burst data; the line refers to the background. [*See the electronic edition of the Journal for a color version of this figure.*]

The last two bursts, GRB 060203 and GRB 060206, are both long bursts triggered by BAT (Barthelmy et al. 2006; Morris et al. 2006). MAGIC data overlap with XRT data on the X-ray afterglow of GRB 060206, immediately after the BAT data, as shown in Figure 4. No evidence of flares or of the jet break have been claimed, but optical observations provided a high redshift value (Palmer et al. 2006; Aoki et al. 2006).

4.2. *GRB 050713a and GRB 050904 Prompt-Emission Observations*

GRB 050713a is of particular interest, being the first burst observed by MAGIC during its prompt emission (Albert et al. 2006). On 2005 July 13 at 04:29:02 UT, the BAT instrument detected a burst located at R.A. = $21^{h}22^{m}09.53^{s}$, decl. = $+77^{\circ}04'29.50'' \pm 3'$ (Falcone et al. 2005). The MAGIC alert system received and validated the alert 13 s after the burst; data taking started 40 s after the burst original time T_0 (Galante et al. 2005). The burst was classified as a bright burst by *Swift* with a duration of $T_{90} = 70 \pm 10$ s. The brightest part of the keV emission occurred within $T_0 + 20$ s, three smaller peaks followed at $T_0 + 50$, $T_0 + 65$, and $T_0 + 105$ s, while a *preburst* peak took place at $T_0 - 60$ s (see Fig. 5). The spectrum, over the interval from $T_0 - 70$ to $T_0 + 121$ s, can be fitted with a power law with photon index -1.58 ± 0.07 and yields a fluence of 9.1×10^{-6} erg cm^{-2} in the 15–350 keV range (Palmer et al. 2005). The burst triggered also the Konus-*Wind* satellite (Golenetskii et al. 2005), which measured the spectrum of the burst during the first 16 s, which is the duration of the first big peak as reported by *Swift*. In the local coordinate system of MAGIC, GRB 050713a was located at an azimuth angle of -6° (near north) and a zenith angle of 50°. The sky region of the burst was observed during 37 minutes, until twilight.

GRB 050904 is also of particular interest, being the second and the latest burst with prompt emission observed by MAGIC. It was triggered at 01:51:44 UT by BAT; the coordinates were R.A. = $0^{h}54^{m}50.79^{s}$, decl. = $+14^{\circ}05'09.42'' \pm 3'$ (Cummings et al. 2005). XRT slewed promptly and started the observation at $T_0 + 161$ s, revealing an uncataloged fading source. It is a long burst ($T_{90} = 225$ s), with a total fluence of 5.4×10^{-6} erg cm^{-2} in the 15–150 keV range (Sakamoto et al. 2005). This burst is the most distant burst ever observed, with an estimated redshift $z = 6.29$ (Kawai et al. 2005). Its X-ray light curve (see Fig. 6) shows a clear X-ray flare at $T_0 + 466$ s (Mineo et al. 2005), and is thus in the MAGIC observation window.

5. RESULTS

All nine GRBs were analyzed using the MAGIC standard analysis described above. In this work the image-cleaning algorithm using also arrival time information was used, as it is more robust. For each GRB a dedicated OFF-source data set was selected on the basis of being compatible with the ON data with respect to several parameters: zenith angle, as the effective area depends strongly on it; local brightness of the sky, depending mostly on Moon phase and zenith angle; and trigger rate, depending mostly on atmospheric transparency and on hardware settings. Loose preliminary cuts were used to remove unphysical events. After training of the RF, for each burst a ''hadronness'' cut was

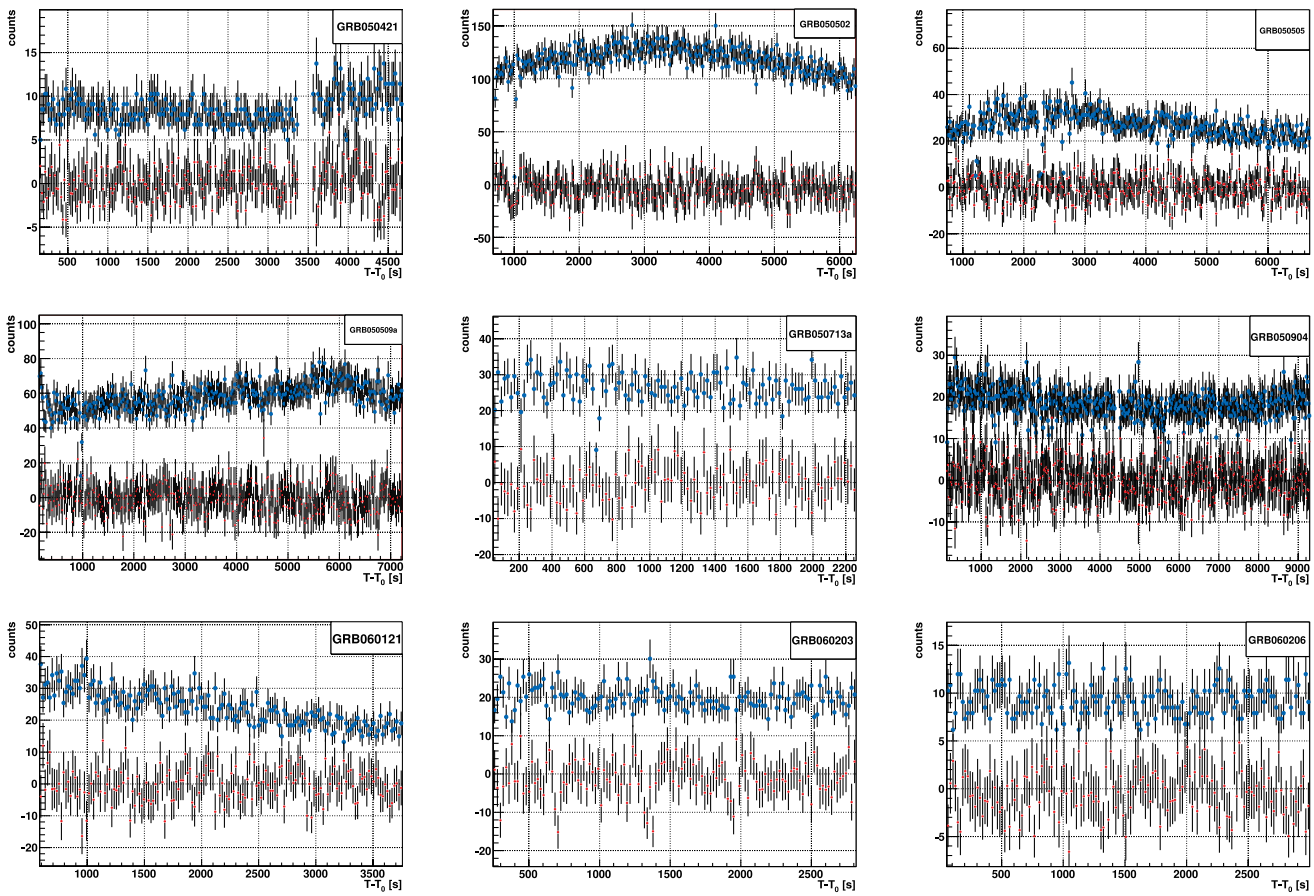

FIG. 8.—Light curves of all nine GRBs for the complete data set of each burst. The background rate of GRB 050502 is particularly high because of a higher night-sky background due to the Moon light.

applied that granted about 90% efficiency on γ-ray events according to the corresponding Monte Carlo, in order to keep high statistics of possible γ-ray events.

The analysis showed no evident signal excess, as can be seen in Figure 7. For each burst the ALPHA plot over the whole data set and for reconstructed energies greater than 100 GeV is shown. The ALPHA distributions of the GRB data sets are flat, as expected from background hadronic events, and are compatible with the corresponding OFF-source data set. No excess in the signal region, i.e., for ALPHA $< 30^{\circ}$, can be seen.

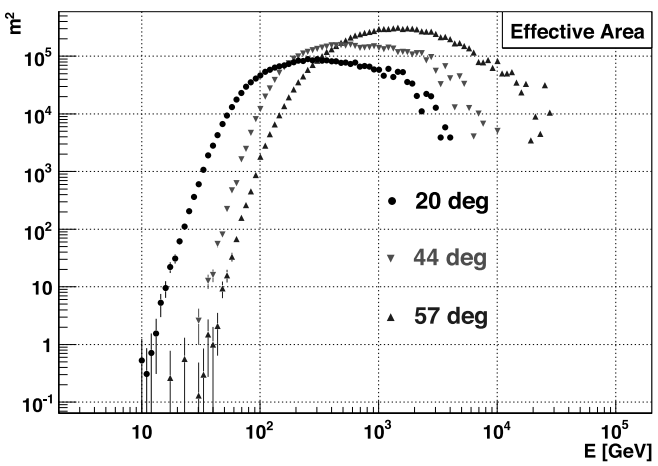

FIG. 9.—Effective area of MAGIC, after typical cuts used in this analysis, for three different zenith angles. [*See the electronic edition of the Journal for a color version of this figure.*]

Nor was any excess seen using a temporal analysis: the entire data-taking interval was divided into 20 s time bins and the number of potential γ-ray events was extracted from the ALPHA distribution; they are shown in the light curves of Figure 8, where red filled circles denote the excess events, and blue open circles the background events (offset by 5 from excess counts in order to make the plot more readable). The distributions of excess events remain zero on average during the observation, and no significant variation of the sample average is visible with time.

Upper limits have been derived for the first 30 minutes of each burst using the Rolke approach (Rolke et al. 2005) in six reconstructed energy bins: 80–120 GeV, 120–175 GeV, 175–225 GeV, 225–300 GeV, 300–400 GeV, and 400–1000 GeV. A systematic uncertainty of 30% on the efficiency has been considered in the upper limit calculation. In every reconstructed energy bin the upper limit in number of excess, calculated with the Rolke approach, has been converted into flux units using the effective area, as explained in the Appendix. The typical effective area of MAGIC for different zenith angles is shown in Figure 9. Table 3 summarizes the upper limits derived for all nine GRBs during the first 30 minutes of data taking.

6. DISCUSSION

A preliminary estimate of the observability of GRBs by the MAGIC telescope had originally been derived using the fourth BATSE catalog (Bastieri et al. 2005; Galante 2006). The GRB

TABLE 3

Derived Fluence Upper Limits for the First 30 Minutes of Data of Nine Gamma-Ray Bursts

Energy Bin (GeV)	Energy (GeV)	Fluence Upper Limit		
		cm^{-2} keV^{-1}	erg cm^{-2}	crab
GRB 050421:				
175–225	212.5	5.26×10^{-16}	3.80×10^{-8}	0.20
225–300	275.8	3.64×10^{-16}	4.43×10^{-8}	0.27
300–400	366.4	5.21×10^{-17}	1.12×10^{-8}	0.08
400–1000	658.7	2.07×10^{-17}	1.41×10^{-8}	0.14
GRB 050502:				
120–175	152.3	1.67×10^{-15}	6.21×10^{-8}	0.27
175–225	219.3	2.83×10^{-15}	2.18×10^{-7}	1.15
225–300	275.8	1.13×10^{-15}	1.37×10^{-7}	0.83
300–400	360.8	7.57×10^{-17}	1.58×10^{-8}	0.11
400–1000	629.1	5.62×10^{-17}	3.56×10^{-8}	0.35
GRB 050505:				
175–225	212.9	2.03×10^{-15}	1.48×10^{-7}	0.76
225–300	275.1	2.66×10^{-15}	3.22×10^{-7}	1.94
300–400	363.6	5.28×10^{-16}	1.11×10^{-7}	0.79
400–1000	704.1	1.85×10^{-17}	1.46×10^{-8}	0.15
GRB 050509a:				
175–225	215.1	1.04×10^{-15}	7.69×10^{-8}	0.40
225–300	273.4	1.39×10^{-15}	1.67×10^{-7}	1.00
300–400	362.8	7.74×10^{-16}	1.63×10^{-7}	1.15
400–1000	668.5	1.69×10^{-16}	1.21×10^{-7}	1.22
GRB 050713a:				
120–175	169.9	3.63×10^{-15}	1.68×10^{-7}	0.76
175–225	212.5	1.12×10^{-15}	8.08×10^{-8}	0.42
225–300	275.8	2.07×10^{-15}	2.52×10^{-7}	1.52
300–400	366.4	3.33×10^{-16}	7.16×10^{-8}	0.51
400–1000	658.7	2.24×10^{-17}	1.55×10^{-8}	0.15
GRB 050904:				
80–120	85.5	9.06×10^{-15}	1.06×10^{-7}	0.32
120–175	140.1	3.00×10^{-15}	9.42×10^{-8}	0.38
175–225	209.9	2.18×10^{-15}	1.53×10^{-7}	0.79
225–300	268.9	5.82×10^{-16}	6.74×10^{-8}	0.40
300–400	355.2	5.01×10^{-16}	1.11×10^{-7}	0.71
400–1000	614.9	1.26×10^{-16}	7.63×10^{-8}	0.73
GRB 060121:				
120–175	151.3	2.64×10^{-15}	9.67×10^{-8}	0.41
175–225	212.8	6.57×10^{-16}	4.76×10^{-8}	0.25
225–300	273.7	2.13×10^{-16}	2.56×10^{-8}	0.15
300–400	367.7	4.47×10^{-16}	9.66×10^{-8}	0.69
400–1000	636.4	4.84×10^{-17}	3.14×10^{-8}	0.31
GRB 060203:				
120–175	151.5	1.10×10^{-14}	4.03×10^{-7}	1.71
175–225	219.5	5.07×10^{-16}	3.91×10^{-8}	0.21
225–300	274.0	1.57×10^{-16}	1.88×10^{-8}	0.11
300–400	365.3	3.54×10^{-16}	7.56×10^{-8}	0.54
400–1000	639.5	4.45×10^{-17}	2.91×10^{-8}	0.29
GRB 060206:				
80–120	85.5	1.23×10^{-14}	1.44×10^{-7}	0.44
120–175	139.9	9.83×10^{-16}	3.08×10^{-8}	0.13
175–225	210.3	5.50×10^{-16}	3.89×10^{-8}	0.20
225–300	269.2	3.65×10^{-16}	4.23×10^{-8}	0.25
300–400	355.4	6.47×10^{-16}	1.31×10^{-7}	0.91
400–1000	614.0	2.88×10^{-17}	1.74×10^{-8}	0.17

Notes.—The first column shows the reconstructed energy bins in which the analysis has been done. The second column shows the true energy at which the upper limits have been calculated, and is the energy giving the average flux upper limit in the reconstructed energy bin. The last column shows the upper limit value in crab units.

spectra were extended to GeV energies with a simple power law and using the observed high-energy spectral index. The extrapolated fluxes were finally compared to the estimated MAGIC sensitivity. Setting conservative cuts on observation times and significances, and assuming an energy threshold of 30 GeV, a 5 σ signal rate of 0.5–2 per year was obtained for an assumed observation delay between 15 and 60 s and a BATSE trigger rate of $\sim$360 per year. Taking into account the rate of GRBs (Guetta et al. 2005) and extrapolating GRB spectra, as observed by BATSE, to VHE using an unbroken power law of reasonable power index (Preece et al. 2000), it was foreseen that MAGIC could detect about one GRB per year at a 5 σ level. A maximal redshift up to $z = 2$ was considered.

This estimate must be revised: the *Swift* alert rate is about a factor 2 lower than predicted, and it includes bursts even fainter than those observed by BATSE; also, for these bursts the effective MAGIC energy threshold at analysis level was higher than the assumed one ($\sim$80 GeV); most important, the distribution of bursts detected by *Swift* has a much higher median redshift than expected. As a result, the number of GRBs that MAGIC can detect is now estimated to lie in the range of 0.2–0.7 per year. This number can be expected to increase again with the launch of *GLAST* and AGILE, and the increased number of alerts due to GRB monitoring by *GLAST*, AGILE, and *Swift* altogether.

7. CONCLUSIONS

MAGIC was able to observe part of the prompt and the early afterglow emission phase of many GRBs as a response to the alert system provided by several satellites. No excess events above $\sim$100 GeV were detected, neither during the prompt-emission phase nor during the early afterglow. We have derived upper limits for the γ-ray flux between 85 and 1000 GeV. These limits are compatible with a naive extension of the power-law spectrum, when the redshift is known, up to hundreds of GeV.

For the first time an atmospheric Cerenkov telescope was able to perform direct rapid observations of the prompt-emission phase of GRBs. This is particularly relevant in the so-called *Swift* era. Although strong absorption of the high-energy γ-ray flux by the MRF is expected at high redshifts, given its sensitivity to low fluxes and its fast-slewing capabilities, the MAGIC telescope is currently expected to detect about 0.5 GRBs per year, if the GRB spectra extend to the energy domain of hundreds of GeV, following a power law with reasonable indices.

The construction of the MAGIC telescope was mainly made possible by the support of the German BMBF and MPG, the Italian INFN, and the Spanish CICYT, to whom goes our grateful acknowledgment. We would also like to thank the IAC for the excellent working conditions at the Observatorio del Roque de los Muchachos in La Palma. This work was further supported by ETH Research Grant TH 34/04 3 and Polish MNiI Grant 1P03D01028.

Facilities: MAGIC

APPENDIX

UPPER LIMIT CALCULATION

The recorded number of events in a particular reconstructed energy bin $\Delta E_{\rm rec}$ is

$$N_{\Delta E_{\rm rec}} = \int_0^\infty \phi(E) A_{\rm eff}(E|\Delta E_{\rm rec})\, dE\, \Delta T, \tag{A1}$$

where $\phi(E)$ is the flux (photons cm^{-2} s^{-1} GeV^{-1}), $A_{\rm eff}(E|\Delta E_{\rm rec})$ is the effective area after all cuts, included the reconstructed energy cut $\Delta E_{\rm rec}$, and ΔT the total time interval of observation. It should be noted that the flux ϕ and the effective area A depend on the *true* energy, while the cuts for the selection of the excess events $N_{\Delta E_{\rm rec}}$ and of the effective area $A_{\rm eff}(E|\Delta E_{\rm rec})$ depend on the reconstructed (estimated) energy. The integral is computed in *true* energy dE.

Being the effective area $A_{\rm eff}(E|\Delta E_{\rm rec})$ depending on energy, we must assume a spectral shape, in our case the typical power law of a GRB:

$$\phi(E) = k \times \left(\frac{E}{E_0}\right)^{\beta}, \tag{A2}$$

where k is a normalization factor (photons cm^{-2} s^{-1} GeV^{-1}), β is the average high-energy power-law index $\beta = -2.5$, and E_0 the pivot energy (e.g., 1 GeV). From equation (A1) we obtain the normalization factor as

$$k_* = \frac{N_{\Delta E_{\rm rec}}}{\int_0^\infty A_{\rm eff}(E|\Delta E_{\rm rec})(E/E_0)^{\beta}\, dE\, \Delta T}. \tag{A3}$$

In our case $N_{\Delta E_{\rm rec}}$ is the upper limit in number of excess events calculated with Rolke statistics. The flux upper limit is

$$\phi_{\rm UL}(E) = k_* \times \left(\frac{E}{E_0}\right)^{\beta}. \tag{A4}$$

The value of the energy E is chosen in a very simple way. We calculate the energy that gives the average flux in the observed reconstructed energy bin:

$$\langle\phi\rangle_{A_{\rm eff}} = \frac{\int_0^\infty \phi(E) A_{\rm eff}(E|\Delta E_{\rm rec})\, dE}{\int_0^\infty A_{\rm eff}(E|\Delta E_{\rm rec})\, dE} = \frac{N_{\Delta E_{\rm rec}}}{\int_0^\infty A_{\rm eff}(E|\Delta E_{\rm rec})\, dE\, \Delta T}. \tag{A5}$$

From equations (A1) and (A3) we can write

$$\langle \phi \rangle_{A_{\rm eff}} = \frac{N_{\Delta E_{\rm rec}}}{\int_0^\infty A_{\rm eff}(E|\Delta E_{\rm rec})(E/E_0)^\beta \, dE} \times \frac{\int_0^\infty A_{\rm eff}(E|\Delta E_{\rm rec})(E/E_0)^\beta \, dE}{\int_0^\infty A_{\rm eff}(E|\Delta E_{\rm rec}) \, dE \, \Delta T} = k_* \left\langle (E/E_0)^\beta \right\rangle_{A_{\rm eff}}. \quad \text{(A6)}$$

Defining $(E_*/E_0) \equiv \langle (E/E_0)^\beta \rangle_{A_{\rm eff}}^{1/\beta}$, from equation (A4) we can calculate the average flux upper limit in the reconstructed energy bin:

$$\phi_{\rm UL}(E_*) = k_* \times \left(\frac{E_*}{E_0}\right)^\beta = \langle \phi_{\rm UL} \rangle_{A_{\rm eff}}. \quad \text{(A7)}$$

Equation (A7) has been used to calculate the upper limits shown in Table 3.

REFERENCES

Albert, J., et al. 2006, ApJ, 641, L9
Aoki, K., et al. 2006, GCN Circ. 4703, http://gcn.gsfc.nasa.gov/gcn/gcn3/4703.gcn3
Arimoto, M., et al. 2006, GCN Circ. 4550, http://gcn.gsfc.nasa.gov/gcn/gcn3/4550.gcn3
Atkins, R., et al. 2000, ApJ, 533, L119
———. 2005, ApJ, 630, 996
Bahcall, J. N., & Mészáros, P. 2000, Phys. Rev. Lett., 85, 1362
Barbier, L. M., et al. 2005a, GCN Circ. 3296, http://gcn.gsfc.nasa.gov/gcn/gcn3/3296.gcn3
———. 2005b, GCN Circ. 3407, http://gcn.gsfc.nasa.gov/gcn/gcn3/3407.gcn3
Barthelmy, S., et al. 2006, GCN Circ. 4656, http://gcn.gsfc.nasa.gov/gcn/gcn3/4656.gcn3
Bastieri, D., et al. 2005, in Proc. 29th Cosmic Ray Conf. (Pune), 4, 435
Beloborodov, A. 2005, ApJ, 618, L13
Böttcher, M., & Dermer, C. D. 1998, ApJ, 499, L131
Breiman, L. 2001, Machine Learning, 45, 5
Bretz, T., et al. (the MAGIC Collaboration). 2003, in Proc. 28th Int. Cosmic Ray Conf. (Tsukuba), 2943
———. 2005, in Proc. 29th Int. Cosmic Ray Conf. (Pune), 4, 315
Burrows, D., et al. 2005, Science, 309, 1833
Chiang, J., & Dermer, C. D. 1999, ApJ, 512, 699
Connaughton, V., et al. 1997, ApJ, 479, 859
Cortina, J., et al. (the MAGIC Collaboration). 2005, in Proc. 29th Int. Cosmic Ray Conf. (Pune), 5, 359
Cummings, J., et al. 2005, GCN Circ. 3910, http://gcn.gsfc.nasa.gov/gcn/gcn3/3910.gcn3
de Jager, O. C., & Stecker, F. W. 2002, ApJ, 566, 738
Derishev, E. V., Kocharovsky, V. V., & Khocarovsky, Vl. V. 1999, ApJ, 521, 640
———. 2001, A&A, 372, 1071
Dermer, C. D., Chiang, J., & Mitman, K. 2000, ApJ, 537, 785
Dingus, B. L. 1995, Ap&SS, 231, 187
Durig, D. T. 2005, IAU Circ. 8521
Falcone, A., et al. 2005, GCN Circ. 3581, http://gcn.gsfc.nasa.gov/gcn/gcn3/3581.gcn3
Fegan, D. J. 1997, J. Phys. G, 23, 1013
Fragile, P., et al. 2004, Astropart. Phys., 20, 591
Galante, N. 2006, Ph.D. thesis, Univ. Studi Siena, http://wwwmagic.mppmu.mpg.de/publications/theses/NGalante.pdf.gz
Galante, N., et al. 2005, GCN Circ. 3747, http://gcn.gsfc.nasa.gov/gcn/gcn3/3747.gcn3
Gaug, M. 2006, Ph.D. thesis, Univ. Autònoma Barcelona, http://magic.mppmu.mpg.de/publications/theses/MGaug.pdf
Gaug, M., et al. (the MAGIC Collaboration). 2005, in Proc. 29th Int. Cosmic Ray Conf. (Pune), 5, 375
Godet, O., et al. 2006, A&A, 452, 819
Golenetskii, S., et al. 2005, GCN Circ. 3619, http://gcn.gsfc.nasa.gov/gcn/gcn3/3619.gcn3
———. 2006, GCN Circ. 4564, http://gcn.gsfc.nasa.gov/gcn/gcn3/4564.gcn3
González, M. M., Dingus, B. L., Kaneko, Y., Preece, R. D., Dermer, C. D., & Briggs, M. S. 2003, Nature, 424, 749
Götting, N., et al. 2003, GCN Circ. 1007, http://gcn.gsfc.nasa.gov/gcn/gcn3/1007.gcn3
Gotz, D., et al. 2005a, GCN Circ. 3323, http://gcn.gsfc.nasa.gov/gcn/gcn3/3323.gcn3
———. 2005b, GCN Circ. 3329, http://gcn.gsfc.nasa.gov/gcn/gcn3/3329.gcn3
Guetta, D., Piran, T., & Waxman, E. 2005, ApJ, 619, 412
Guetta, D., et al. 2007, A&A, 461, 95
Hengstebeck, T. 2006, Ph.D. thesis, Humboldt Univ. Berlin
Hillas, A. M. 1985, in Proc. 19th Int. Cosmic Ray Conf. (La Jolla), 3, 445
Horan, D., et al. 2007, ApJ, 655, 396
Hullinger, D., et al. 2005, GCN Circ. 3364, http://gcn.gsfc.nasa.gov/gcn/gcn3/3364.gcn3
Hurkett, C., et al. 2005a, GCN Circ. 3360, http://gcn.gsfc.nasa.gov/gcn/gcn3/3360.gcn3
———. 2005b, GCN Circ. 3379, http://gcn.gsfc.nasa.gov/gcn/gcn3/3379.gcn3
Hurley, K., et al. 1994, Nature, 372, 652
Jarvis, B., et al. (the STACEE Collaboration). 2005, in Proc. 29th Int. Cosmic Ray Conf. (Pune), 4, 455
Kawai, N., et al. 2005, GCN Circ. 3937, http://gcn.gsfc.nasa.gov/gcn/gcn3/3937.gcn3
Kobayashi, S., Zhang, B., Mészáros, P., & Burrows, D. 2007, ApJ, 655, 391
Levan, A. J., et al. 2006, GCN Circ. 4841, http://gcn.gsfc.nasa.gov/gcn/gcn3/4841.gcn3
Li, Z., Dai, G., & Lu, T. 2002, A&A, 396, 303
Malesani, D., et al. 2006, GCN Circ. 4561, http://gcn.gsfc.nasa.gov/gcn/gcn3/4561.gcn3
Mangano, V., et al. 2006, GCN Circ. 4565, http://gcn.gsfc.nasa.gov/gcn/gcn3/4565.gcn3
Mannheim, K., Hartmann, D., & Burkhardt, F. 1996, ApJ, 467, 532
Mereghetti, S., & Mowlavi, N. 2005, GCN Circ. 4084, http://gcn.gsfc.nasa.gov/gcn/gcn3/4084.gcn3
Mészáros, P. 2006, Rep. Prog. Phys., 69, 2259
Mészáros, P., Rees, M., & Papathanassoiu, H. 1994, ApJ, 432, 181
Mineo, T., et al 2005, GCN Circ. 3920, http://gcn.gsfc.nasa.gov/gcn/gcn3/3920.gcn3
Mirzoyan, R., et al. (the MAGIC Collaboration). 2005, in Proc. 29th Int. Cosmic Ray Conf. (Pune), 4, 23
Morris, D., et al. 2006, GCN Circ. 4682, http://gcn.gsfc.nasa.gov/gcn/gcn3/4682.gcn3
———. 2007, ApJ, 654, 413
Nikishov, A. I. 1961, Zh. Eksp. Teor. Fiz., 41, 549 (English transl. in Soviet Phys.-JETP Lett., 14, 392 [1962])
Padilla, L., et al. 1998, A&A, 337, 43
Palmer, D., et al. 2005, GCN Circ. 3597, http://gcn.gsfc.nasa.gov/gcn/gcn3/3597.gcn3
———. 2006, GCN Circ. 4697, http://gcn.gsfc.nasa.gov/gcn/gcn3/4697.gcn3
Papathanassiou, H., & Mészáros, P. 1996, ApJ, 471, L91
Pe'er, A., & Waxman, E. 2004, ApJ, 613, 448
Pilla, R. P., & Loeb, A. 1998, ApJ, 494, L167
Piran, T. 1999, Phys. Rep., 314, 575
Poirier, J., et al. 2003, Phys. Rev. D, 67, 042001
Preece, R. D., Briggs, M. S., Mallozzi, R. S., Pendleton, G. N., Paciesas, W. S., & Band, D. L. 2000, ApJS, 126, 19
Razzaque, S., Mészáros, P., & Zhang, B. 2004, ApJ, 613, 1072
Rolke, W., López, A., & Conrad, J. 2005, Nucl. Instrum. Methods Phys. Res. A, 551, 493
Rossi, E., Beloborodov, A., & Rees, M. J. 2006, MNRAS, 369, 1797
Sakamoto, T., et al. 2005, GCN Circ. 3938, http://gcn.gsfc.nasa.gov/gcn/gcn3/3938.gcn3
Saz Parkinson, P., et al. 2006a, in AIP Proc. 836, Gamma Ray Bursts in the *Swift* Era, ed. S. S. Holt, N. Gehrels, & J. A. Nousek (New York: AIP), 624
———. 2006b, GCN Circ. 5527, http://gcn.gsfc.nasa.gov/gcn/gcn3/5527.gcn3
———. 2007, Nuovo Cimento, in press (astro-ph/0611457)
Scapin, V., et al. 2007, Nuovo Cimento, in press
Totani, T. 2000, ApJ, 536, L23
Wang, X., Dai, Z., & Lu, T. 2001, ApJ, 556, 1010
Wang, X., Li, Z., & Mészáros, P. 2006, ApJ, 641, L89
Waxman, E. 1995, Phys. Rev. Lett., 75, 386
Zhang, B., & Mészáros, P. 2001, ApJ, 559, 110
Zhou, X., et al. 2003, in Proc. 28th Int. Cosmic Ray Conf. (Tsukuba), 2757